This is the preprint of an article published, in revised form, in
Separation and Purification Technology, vol. 215, pp. 548–556 (2019). doi:10.1016/j.seppur.2019.01.051

Consideration of the Joule-Thomson effect for the transport of vapor through anodic alumina membranes under conditions of capillary condensation

Thomas Loimer[a,*], Katerina Setnickova[b], Petr Uchytil[b]

[a] *Institute of Fluid Mechanics and Heat Transfer, TU Wien, 1060 Vienna, Austria*
[b] *Institute of Chemical Process Fundamentals, Academy of Sciences of the Czech Republic, 165 02 Prague, Czech Republic*

Abstract

Anodic alumina membranes have straight pores and a very uniform pore size distribution. Data on the permeance for the flow of isobutane vapors through anodic alumina membranes with pore diameters between 20 nm and 90 nm has been reported recently [Petukhov et al., J. Phys. Chem. C 120, 10982–10990, 2016]. For the upstream pressure approaching the saturation pressure, a sudden increase of the permeance was observed. Taking into account capillary condensation and assuming isothermal conditions within the entire flow field, the permeance data was used to compute the radii of curvature of the menisci separating the liquid condensate from the vapor.

In the present work, the radius of curvature of the meniscus within the membrane is set to the pore radius. The permeance is computed for (i) isothermal flow and, taking into account the energy balance and the real fluid properties of isobutane, i.a., the Joule-Thomson effect, for (ii) adiabatic and (iii) diabatic conditions at the downstream side of the membrane.

The predicted permeances depend significantly on the temperature variation within the flow field. From a comparison of the predicted permeances with the data reported by Petukhov *et al.*, it is concluded that heat transfer should be taken into account to model the flow of vapors through anodic alumina membranes in case that condensation occurs.

Keywords: mass flow, inorganic membranes, porous media, capillary condensation, Joule-Thomson effect

1. Introduction

Anodic alumina membranes possess a very regular structure consisting of round, straight pores, which are regularly distributed in plane sheets of the membrane material and which have a narrow distribution of the pore diameter [1, 2]. The distance between pores is of the order of the pore diameter, yielding void fractions of the anodic alumina membranes between 17% and 30%. Petukhov *et al.* [1] produced membranes with thicknesses of 100 μm and pore diameters between 20 nm and 90 nm. They measured permeances of permanent gases and of isobutane through these membranes. For a feed pressure of the isobutane larger than approx. 0.9 times the saturation pressure, the permeance increased considerably. The increase of the mass flux was attributed to condensation of the isobutane vapor within the membrane, i.e., to capillary condensation. Petukhov *et al.* [1] applied an isothermal description of the flow to compute the radius of curvature of the meniscus within the membrane from the permeance data. In part, they obtained meniscus radii which were smaller than the pore radius. The present investigation attempts to explain this result

The flow of vapors through micro-porous membranes under conditions where capillary condensation occurs was investigated by a number of researchers [3–7]. Rhim & Hwang [3] proposed a criterion for the occurrence of capillary condensation by applying Kelvin's equation, and a description of the flow under conditions of capillary condensation based, inter alia, on Kelvin's equation and on Young-Laplace's equation. Kelvin's equation relates the pressure of a vapor that is in equilibrium with its liquid phase above a curved meniscus to the saturation pressure. The Young-Laplace equation gives the pressure difference across a curved meniscus. Rhim & Hwang [3], as well as the other authors mentioned above [4–7] modeled the porous membranes to consist of round pores, where all pores have the same pore diameter. The flow field under conditions of capillary condensation is visualized as sketched in Fig. 1.

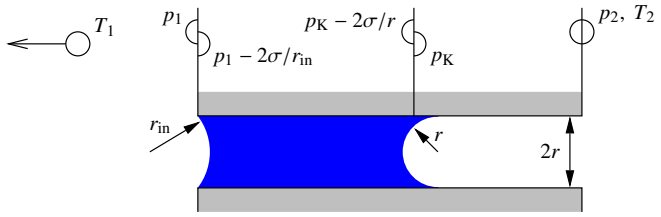

Figure 1: Flow field under conditions of capillary condensation in a single pore. Here, the radius of curvature of the meniscus within the pore is set equal to the pore radius.

Regarding the part of the membrane filled with condensate, Rhim & Hwang [3] observed that the enthalpy of vaporization released by condensation at the upstream meniscus must be primarily transported by heat conduction to the downstream

*Corresponding author
Email addresses: thomas.loimer@tuwien.ac.at (Thomas Loimer), setnickova@icpf.cas.cz (Katerina Setnickova), uchytil@icpf.cas.cz (Petr Uchytil)

meniscus, where it is consumed for evaporation. Hence, they stated, "*Thus, a finite temperature distribution always exists even though the system is kept in an isothermal bath.*" [3, p. 176]. In their description of the flow, Rhim & Hwang [3] took account of a temperature variation within the flow field. However, later authors assumed isothermal conditions [4–7] throughout the entire flow field.

In the studies cited above, Vycor glass membranes with pore diameters between 2 nm and 4 nm [3–5, 7] or γ-alumina membranes with pore sizes of 3 nm [6] were used. For these pore sizes, in the studies above account was also taken of surface flow, i.e., the flow of a layer of adsorbate along the pore walls [8]. For a slightly larger pore sizes, for instance, investigating the flow of nitrogen at 77 K through a track-etched membrane with a pore size of 10 nm [9], surface flow was not taken into account.

While, in reality, the pore space in these materials is of irregular shape, a model of the porous medium consisting of straight pores was used. With respect to the resistance of the porous medium to molecular flow, viscous flow of the gaseous phase, or viscous flow of the liquid phase of the fluid, the irregular pore shape can be readily related to an equivalent bundle of straight capillaries, for instance by using permeation data of a non-condensing gas. The outcome of such permeation data would be an effective pore diameter of the straight pores. However, if effects of capillarity, for instance the pressure drop across menisci, are also taken into account, the relation between the pore size and an effective pore diameter of round, straight pores is not so clear. The description of the porous medium as consisting of straight pores is obviously better suited for, e.g., track-etched membranes [9] or anodic alumina membranes [1].

The flow of a fluid through a porous material can also be regarded as a throttling process. In an adiabatic throttling process, the enthalpy of the fluid is the same at the upstream as at the downstream location. In this case, for real fluids the Joule-Thomson effect is recovered. Schneider [10] investigated the flow of a saturated vapor through a porous material, without considering capillary condensation. While a gas might become warmer in a Joule-Thomson process, a vapor always cools down. The temperature difference across the membrane causes a transfer of heat in downstream direction. However, the saturated vapor upstream of the membrane can only release heat by condensation. Therefore, the vapor upstream of the membrane must condense partially or fully. The state of the fluid at the downstream location is an unsaturated vapor, therefore any condensate must evaporate before it reaches the downstream location of the membrane. In effect, due to the Joule-Thomson effect, a saturated vapor that flows through a porous medium condenses fully or partially, regardless of whether the liquid phase of the fluid wets or does not wet the membrane material.

One result of the analysis of Schneider [10] is, that the vapor condenses completely if the pore size of the porous medium is below a certain value. Otherwise, the vapor condenses partially. For partial condensation, the mass flux through the porous material is nearly the same as the mass flux of the gaseous phase through the porous material. If complete condensation occurs, the mass flux is increased with respect to the mass flux of the gaseous phase.

The analysis of Schneider [10] was later extended by allowing unsaturated vapors and accounting for capillary condensation [11]. Using an adiabatic description, the flow of butane and isobutane vapors through porous Vycor glass with pore sizes between 20 nm and 200 nm [11] and through asymmetric, ceramic membranes with a pore size of the separation layer of 20 nm [12] were investigated. In these studies, a Matlab [13] code for computing the mass flow through homogeneous and multi-layered membranes was developed. Engineering correlations for the material properties of the fluid and the membrane were implemented and the governing equations were solved fully numerically [11, 14].

For the present work, this code was modified to (i) solve for isothermal flow conditions and (ii) to allow not only adiabatic, but also diabatic boundary conditions. Given a contact angle of the liquid phase of the fluid on the membrane material, the upstream pressure and temperature and the downstream pressure of the fluid, the result of the computations is the mass flux through the membrane. This result is not compared directly with the result of Petukhov *et al.* [1]: They applied a simplified, algebraic description of the flow and, given the mass flux, obtained the radius of curvature of the meniscus within the membrane.

2. Theory

Within the flow field, the balances of mass, momentum and energy must be satisfied [11],

$$\dot{m} = \text{constant}, \tag{1}$$

$$\dot{m} = -\frac{\kappa}{\nu}\frac{\mathrm{d}p}{\mathrm{d}z}, \tag{2}$$

$$\dot{m}h + \dot{q} = \text{constant}, \tag{3}$$

where $\dot{m}$ is the mass flux, κ refers to the permeability of the membrane, ν denotes the kinematic viscosity of the fluid, p refers to the pressure, the spatial coordinate in flow direction is given by z, the specific enthalpy of the fluid is given by h and $\dot{q}$ refers to the heat flux. Note, that as the momentum balance D'Arcy's equation is used, which is valid for a purely viscous flow through a porous medium. To account for molecular flow, an effective viscosity of the fluid is introduced. The details are given further below. In the energy balance, the kinetic energy of the fluid is neglected, as is appropriate for a throttling process.

Modeling the porous medium as a bundle of parallel capillaries, the permeability is related to the pore radius by

$$\kappa = \frac{\epsilon}{\tau}\frac{r^2}{8}, \tag{4}$$

where ϵ is the void fraction, τ the tortuosity, and r is the pore radius. To account for molecular flow, the effective kinematic viscosity of the gaseous phase of the fluid is taken to be

$$\nu = \nu_\mathrm{g}(1 + \beta Kn)^{-1}, \tag{5}$$

where ν_g is the kinematic viscosity of the gaseous phase in the bulk, β is a correction factor for molecular flow, and Kn is the Knudsen number. The Knudsen number is given by

$$Kn = \frac{\lambda}{2r}, \tag{6}$$

where λ is the mean free path. From the kinetic theory of gases, the mean free path can be estimated from the kinematic viscosity [15],

$$\lambda = \frac{3\nu_g}{2}\sqrt{\frac{\pi\mathcal{M}}{2\mathcal{R}T}}, \tag{7}$$

where $\mathcal{R}$ and $\mathcal{M}$ refer to the universal gas constant and to the molar mass, respectively, and T is the absolute temperature.

The molecular flow correction factor is taken to be

$$\beta = \frac{256}{9\pi}. \tag{8}$$

For this value of β, substituting from Eqs. (4) to (8) into the momentum balance, Eq. (2), using the ideal gas law and integrating yields a more common form of the momentum equation, confer Eq. (5) in Ref. [16],

$$J = \frac{\epsilon 2r}{3\mathcal{R}TL}\sqrt{\frac{8\mathcal{R}T}{\pi\mathcal{M}}}(p_1 - p_2) + \frac{\epsilon r^2(p_1^1 - p_2^2)}{16\mathcal{R}TL\eta}.$$

Here, J is the molar flux, L is the thickness of the membrane and η denotes the dynamic viscosity. In the present work, the momentum balance as given by Eq. (2) is used, and it is numerically integrated. For example, the density of the gaseous phase of the fluid is given by a virial equation, not by the ideal gas law.

The heat flux $\dot{q}$ is given by Fourier's law of heat conduction,

$$\dot{q} = -k\frac{\mathrm{d}T}{\mathrm{d}z}, \tag{9}$$

where k is the effective thermal conductivity of the fluid-filled membrane. The effective thermal conductivity is computed for a purely parallel orientation of the boundaries between the different media to the heat flux,

$$k = (1 - \epsilon)k_m + \epsilon k_f. \tag{10}$$

Here, k_f and k_m refer to the thermal conductivities of the fluid and the solid matrix of the membrane, respectively.

It is assumed, that the liquid phase of the fluid ideally wets the solid membrane material. Hence, at interfaces within the porous medium, the pressure difference across a meniscus is given by

$$\Delta p = 2\sigma/r, \tag{11}$$

where σ refers to the surface tension. The pressure of the gaseous phase of the fluid that is in equilibrium with its liquid phase at a curved meniscus is denoted by p_K, and it is given by Kelvin's equation,

$$\ln\left(\frac{p_K}{p_{sat}}\right) = -\frac{2\sigma}{r}\frac{v_l\mathcal{M}}{\mathcal{R}T}. \tag{12}$$

Here, v_l is the specific volume of the liquid, and p_{sat} refers to the saturation pressure.

At the upstream front of the membrane, the vapor must condense if the upstream pressure is larger than the pressure p_K, cf. Eq. (12). In that case, Eq. (12) yields the radius of curvature of the meniscus located at the upstream front of the membrane by setting p_K equal to the upstream pressure and solving for r,

$$\ln\left(\frac{p_1}{p_{sat}}\right) = -\frac{2\sigma}{r_{in}}\frac{v_l\mathcal{M}}{\mathcal{R}T}. \tag{13}$$

Here, p_1 is the upstream pressure and r_{in} denotes the radius of curvature of the upstream meniscus.

At curved interfaces, the states of the fluid at both sides of the interface are different from the respective states of the fluid at a plane interface. Therefore, the enthalpy of vaporization at a curved interface is different from the enthalpy of vaporization at a plane interface, and it is given by [17]

$$\Delta h_{vap,K} = \Delta h_{vap} + (p_K - p_{sat})\left(\frac{\partial h_g}{\partial p}\right) - \left(p_K - p_{sat} - \frac{2\sigma}{r}\right)\left(\frac{\partial h_l}{\partial p}\right). \tag{14}$$

Here, $\Delta h_{vap,K}$ and Δh_{vap} refer to the enthalpies of vaporization at a curved interface and at a plane interface, respectively.

The properties of the fluid are given by engineering correlations depending, in general, on temperature and pressure. These correlations are listed in the appendix.

2.1. Isothermal description

Under the assumption of isothermal flow, the energy balance and equations related to heat flux are unnecessary. Hence, the equations governing isothermal flow consist of Eqs. (1), (2), (4) to (8), and (11) to (13).

The boundary conditions are given by prescribing the pressures at the locations of the upstream and the downstream front of the membrane,

$$p(z = 0) = p_1, \tag{15}$$

$$p(z = L) = p_2. \tag{16}$$

Here, p_2 is the downstream pressure.

The momentum equation, Eq. (2), is an ordinary differential equation. The solution to the isothermal description is obtained by constructing an initial value problem from the boundary value problem. Starting from the downstream state, Eq. (2) is integrated in upstream direction, setting the mass flux $\dot{m}$ to an arbitrary value. During integration, the state of the fluid must be checked and, if necessary, an interface with the appropriate jump conditions, Eqs. (11) and (12) is introduced. Integration continues in the other phase. The integration is repeated, modifying $\dot{m}$, until the pressure at the upstream location is equal to the upstream pressure within a tolerance of one thousandths of the pressure difference $p_1 - p_2$. The algorithm is implemented as a Matlab-program [13], using a standard Runge-Kutta solver for integration. Here, the integration in upstream direction is chosen only for convenience. The program to solve for the isothermal description was adapted from the already existing program that solved for the adiabatic description. For the adiabatic description, the integration in upstream direction increased the accuracy of the solution and reduced the complexity and the runtime of the program [18].

2.2. Adiabatic and diabatic descriptions

The adiabatic and diabatic descriptions differ in only one boundary condition at the downstream side of the membrane. For the adiabatic description, zero heat flux is required at the downstream front of the membrane,

$$\dot{q}(z = L) = 0. \tag{17}$$

For the diabatic description, the temperature at the downstream front of the membrane is given, and it is set equal to the upstream temperature,

$$T(z = L) = T_1. \tag{18}$$

For both descriptions, the pressure at the downstream front of the membrane is given,

$$p(z = L) = p_2. \tag{19}$$

At the upstream side, for both descriptions it is assumed that the working fluid and the apparatus are well in thermal equilibrium. Hence, for both descriptions there is no heat flux at the upstream side of the membrane. There may be a temperature boundary layer upstream of the membrane, therefore the upstream boundary conditions must be partially applied at minus infinity,

$$p(z = 0) = p_1, \quad T(z \to -\infty) = T_1, \quad \dot{q}(z \to -\infty) = 0. \tag{20}$$

With these conditions, the system of equations for the adiabatic and the diabatic description is complete. The two ordinary differential equations, Eqs. (2) and (3) must be solved subject to the boundary conditions. As before, an initial value problem is constructed and a shooting method is used to integrate Eqs. (2) and (3) in upstream direction, using the mass flux $\dot{m}$ as a parameter. The criterion for solution is, that the pressure at the upstream front is equal to the upstream pressure within a tolerance of one thousandth of $p_1 - p_2$.

For the adiabatic description, the downstream state of the fluid is not known, since the downstream temperature is not given. The downstream temperature is computed by integrating the Joule-Thomson coefficient along an isenthalpic line

$$T_1 - T_2 = \int_{p_2}^{p_1} \mu_{\mathrm{JT}} \, \mathrm{d}p, \quad \mu_{\mathrm{JT}} = -\frac{(\partial h/\partial p)_T}{c_p}, \tag{21}$$

where μ_{JT} is the Joule-Thomson coefficient and T_2 refers to downstream temperature. The temperature difference is usually very well approximated by

$$T_1 - T_2 = \mu_{\mathrm{JT}}(p_1 - p_2).$$

Vapors always have a positive Joule-Thomson coefficient, therefore, the downstream temperature for the flow of a vapor through a porous membrane is always smaller than the upstream temperature.

For the diabatic description, to have the downstream temperature being equal to the upstream temperature, a heat flux is imposed at the downstream front of the membrane. The necessary heat flux, $\dot{q}_2$, is computed by applying the energy balance between locations far upstream and at the downstream front of the membrane, where the upstream and the downstream states are attained,

$$\dot{m}h_1 = \dot{m}h_2 + \dot{q}_2. \tag{22}$$

The enthalpy difference $h_1 - h_2$ is computed by integrating along an isothermal line, $\mathrm{d}h = (\partial h/\partial p)_T \, \mathrm{d}p$.

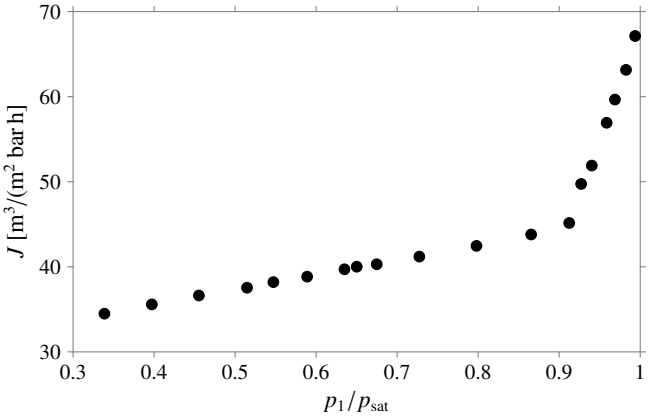

Figure 2: Permeance reported in Ref. [1]. Data taken from the supporting information.

3. Results and discussion

Petukhov *et al.* [1] report permeance data for the flow of isobutane through anodic alumina membranes with pore diameters between 20 nm and 90 nm, see their Fig. 3 and the supplemental information to Ref. [1]. Here, the predictions from the isothermal, adiabatic and diabatic descriptions presented above are compared with the data for their membrane sample AAo_40nm. For the predictions, a pore diameter of 37 nm and a membrane thickness of 100 µm is used. It is sufficient to compare the predictions for one of the membrane samples with experimental data to draw important conclusions.

The dependence of the permeance on the relative upstream pressure, p_1/p_{sat} for the sample AAo_40nm is re-plotted here in Fig. 2. The increase of the permeance with increasing upstream pressure for $p_1/p_{\mathrm{sat}} < 0.9$ suggests that the gaseous phase of the fluid is partially transported by viscous flow. Estimating possible values of the mean pressure from p_1, an appreciable value for the permeance is obtained when extrapolating the line of permeance over mean pressure to a mean pressure of zero. This indicates that molecular flow significantly contributes to the mass transport through the membrane.

The kink at $p_1/p_{\mathrm{sat}} \approx 0.9$ in the plot of permeance versus p_1/p_{sat} probably indicates the onset of capillary condensation. The increase of the permeance with increasing upstream pressure is much larger for $p_1/p_{\mathrm{sat}} > 0.9$ than for $p_1/p_{\mathrm{sat}} > 0.9$. This is the flow enhancement due to capillary condensation.

Figure 3 shows the comparison of the predictions for the permeance according to the isothermal, adiabatic and diabatic descriptions with the experimental data. For values of the upstream pressure far from saturation, all three predictions yield the same value for the permeance. The predicted values are

smaller than the measured values. However, it should be noted that here no fitting parameters are used. Usually, the permeance data for the flow of a non-condensable gas is used to determine the values of, for instance, ϵ/τ and β. Here, these quantities are left at their canonical values, $\tau = 1$ and $\beta = 9.054$, cf. Eqs. (4) and (8).

According to the isothermal description, the onset of capillary condensation occurs at larger values for p_1/p_{sat} than the experimental data seems to indicate. For $p_1 \approx p_{sat}$, the isothermal description predicts a permeance which is approximately three times larger than the measured value.

The increase of the mass flux under conditions of capillary condensation is owed to the difference of the pressure differences across the upstream and the downstream menisci. At the onset of capillary condensation, the radius of curvature of the upstream meniscus is equal to the pore radius. The radius of curvature of the downstream meniscus is also equal to the pore radius, hence these two pressure differences balance each other. Conversely, for p_1 approaching p_{sat}, the radius of curvature of the upstream meniscus becomes much larger than the pore radius. Hence, the pressure difference across the downstream meniscus is much larger than the pressure difference across the upstream meniscus. Therefore, a large additional pressure difference acts to increase the mass flow rate. See the pressure distribution for $p_1/p_{sat} = 0.994$ according to the isothermal description plotted in Fig. 4.

From another point of view, if the isothermal description is used to determine the radius of curvature of the meniscus within the membrane, it can be inferred from the prediction for the permeance that, at $p_1/p_{sat} \approx 0.96$, the radius of curvature of the meniscus within the membrane is equal to the pore radius. For the experimental data points with capillary condensation at values of $p_1/p_{sat} < 0.96$, the radius of curvature of the meniscus within the membrane becomes smaller than the pore radius, at values of $p_1/p_{sat} > 0.96$ it becomes larger than the pore radius.

The adiabatic description predicts the onset of capillary condensation already for a vapor at the upstream side of the membrane rather far from saturation. The permeance predicted for $p_1 \approx p_{sat}$ is slightly smaller than according to the isothermal description. These properties are owed to the temperature distribution. For $p_1/p_{sat} = 0.994$ the temperature and pressure distribution according to the adiabatic description is presented in Fig. 5. The temperature at the upstream front is increased slightly. Therefore, the radius of curvature of the upstream meniscus must decrease, and the pressure difference across the upstream meniscus increases, see the pressure distribution plotted in Fig. 5. According to the diabatic description, the temperature at the upstream front of the membrane is still larger than according to the adiabatic description, and also the pressure difference across the upstream meniscus is larger, see Fig. 6. For the case plotted in Fig. 6, the heat flux supplied to the downstream front of the membrane is $\dot{q} = 1010$ W/m^2.

According to the adiabatic description, condensation already occurs for values of $p_1/p_{sat} > 0.8$. For the range $0.8 < p_1/p_{sat} < 0.98$ a temperature distribution is not shown, but from the permeance data, it must be concluded that in this range the temperature at the upstream front of the membrane is smaller than the upstream temperature.

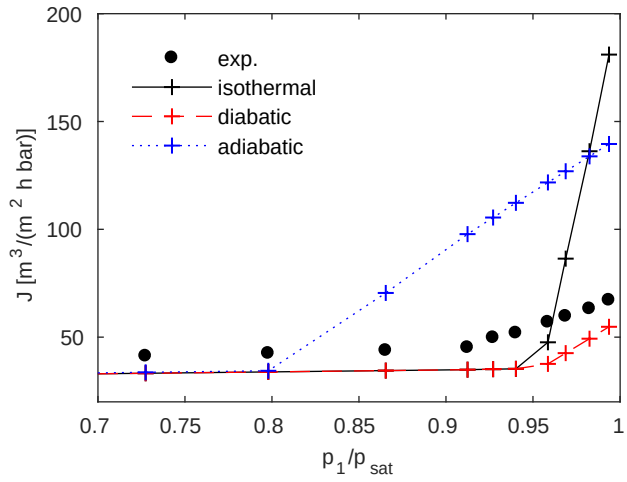

Figure 3: Permeances obtained from experiment and according to the isothermal, diabatic and adiabatic descriptions.

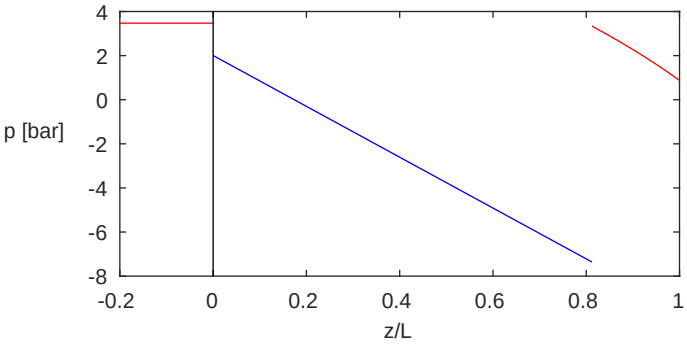

Figure 4: Pressure distribution according to the isothermal description for $p_1/p_{sat} = 0.994$. The red and blue color indicate the flow of the gaseous and the liquid phase, respectively.

While the adiabatic description corresponds to zero heat flux at the downstream front of the membrane, the diabatic description has a heat flux imposed such that the temperature at the downstream front of the membrane is equal to the upstream temperature, or probably equal to the temperature of the surrounding. In other words, the heat transfer coefficient at the downstream side of the membrane is varied between zero for the adiabatic description to infinity for the diabatic description. Looking at the permeance data plotted in Fig. 3, it may happen that for a realistic heat transfer coefficient the experimental data is quite well described.

4. Conclusions

The flow of isobutane vapors through anodic alumina membranes under conditions of capillary condensation was computed according to three theoretical descriptions. These descriptions are derived from first principles and are based on sound assumptions. It is shown, that the temperature distribution plays an important role for the mass transport. Since the difference between the adiabatic and the diabatic description is

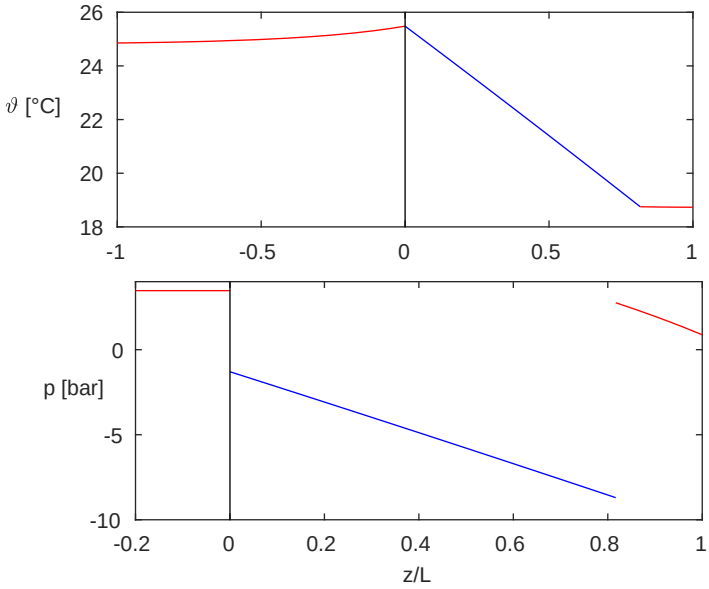

Figure 5: Temperature (top) and pressure distribution (bottom) according to the adiabatic description for $p_1/p_{sat} = 0.994$.

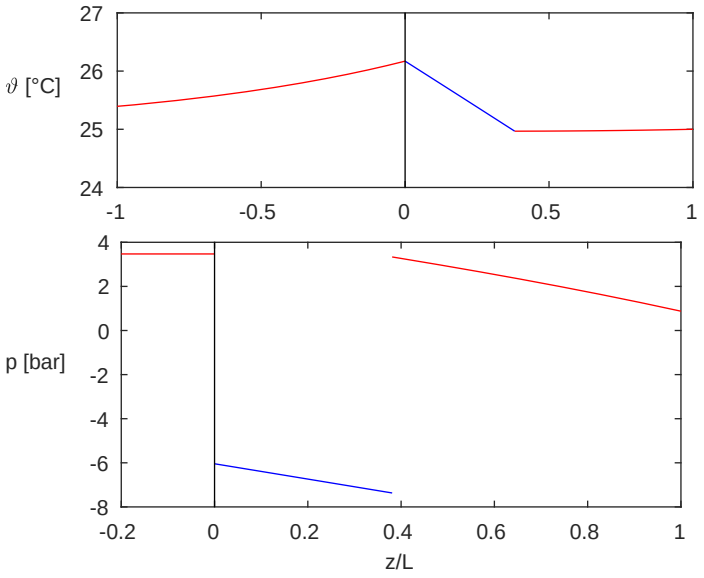

Figure 6: Temperature (top) and pressure distribution (bottom) according to the diabatic description for $p_1/p_{sat} = 0.994$.

a heat flux from the downstream side of the membrane, and from the temperature distributions for these two descriptions, it is concluded that, when condensation occurs, heating the membrane from the downstream side decreases the mass flux. Vice versa, cooling of the downstream side of the membrane could increase the mass flux. While it is obvious that heating or cooling matters for a process with condensation, the influence on the mass flux was probably less obvious.

None of the theoretical predictions agree very well with the data. It may be possible to find a heat transfer coefficient such that the experimental data and the prediction agrees very well, but no attempt was made to find the value of this heat transfer coefficient.

A model of the flow equivalent to the isothermal description presented here was used to compute the radius of curvature of the meniscus within the membrane. Inferring from the permeance data computed here, the determination of the radius of curvature of the meniscus within the membrane is ambiguous as long as the temperature distribution is not known. In order to determine the radius of curvature of the menisci, at least the temperature at the downstream front of the membrane, and probably also the temperatures at the upstream front and far upstream of the membrane are necessary.

Acknowledgements

Funding: This work was supported by AIC Androsch International Management Consulting GmbH.

Appendix A. Material properties

Anodic alumina

Thermal conductivity [19],

$$k_\mathrm{m} = 1.22\ \mathrm{W/m\,K}. \tag{A.1}$$

Isobutane

Molar mass, critical temperature and critical pressure [20],

$$\mathcal{M} = 58.124\ \mathrm{kg/kmol}, \quad T_\mathrm{c} = 408.2\ \mathrm{K}, \quad p_\mathrm{c} = 3.65 \times 10^6\ \mathrm{Pa}. \tag{A.2}$$

The specific volume of the gaseous phase is given by a viral equation,

$$\frac{p\tilde{v}}{\mathcal{R}T} = 1 + \frac{\tilde{B}}{\tilde{v}}, \tag{A.3}$$

where a tilde denotes molar quantities and $\tilde{B}$ is the first virial coefficient [21],

$$\frac{\tilde{B}}{\mathrm{cm^3/mol}} = 116.25 - \frac{1.0293 \times 10^5}{T/\mathrm{K}} - \frac{1.2475 \times 10^7}{(T/\mathrm{K})^2} - \frac{7.049 \times 10^9}{(T/\mathrm{K})^3}. \tag{A.4}$$

Density of the liquid phase [22],

$$\frac{\rho_\mathrm{l}}{\mathrm{kg/m^3}} = 870.93 - 1.36494\frac{T}{\mathrm{K}} + 2.56419 \times 10^{-3}\left(\frac{T}{\mathrm{K}}\right)^2 - 5.32743 \times 10^{-6}\left(\frac{T}{\mathrm{K}}\right)^3. \tag{A.5}$$

Saturation pressure [23],

$$\frac{p_\mathrm{sat}}{\mathrm{Pa}} = 10\hat{}\left(9.00272 - \frac{947.54}{T/\mathrm{K} - 24.28} + 0.43429\chi^{2.6705} - 19.64\chi^8 + 2792\chi^{12}\right), \qquad \chi = \frac{T/\mathrm{K} - 268}{407.1}. \tag{A.6}$$

Molar isobaric heat capacity in the ideal gas state and for the liquid phase [24],

$$\frac{\tilde{c}_{p,\mathrm{id}}}{\mathrm{J/kmol\,K}} = 65490 + 2.4776 \times 10^5\left(\frac{\Theta_1}{\sinh\Theta_1}\right)^2 + 1.575 \times 10^5\left(\frac{\Theta_2}{\cosh\Theta_2}\right)^2, \qquad \Theta_1 = \frac{1587}{T/\mathrm{K}}, \quad \Theta_2 = -\frac{706.99}{T/\mathrm{K}}, \tag{A.7}$$

$$\frac{\tilde{c}_{p,\mathrm{l}}}{\mathrm{J/kmol\,K}} = 1.7237 \times 10^5 - 1.7839 \times 10^3 T/\mathrm{K} + 14.759(T/\mathrm{K})^2 - 4.7909 \times 10^{-2}(T/\mathrm{K})^3 + 5.805 \times 10^{-5}(T/\mathrm{K})^4. \tag{A.8}$$

Dynamic viscosity of the gaseous phase [20],

$$\frac{\eta\mathrm{g}}{\mathrm{Pa\,s}} = \left(0.807T_\mathrm{r}^{0.618} - 0.357\exp\left(-0.449T_\mathrm{r}\right) + 0.34\exp\left(-4.058T_\mathrm{r}\right) + 0.018\right)\mathcal{M}^{1/2}p_\mathrm{c}^{2/3}\left(T_\mathrm{c}\mathcal{R}N_\mathrm{Avo}^2\right)^{-1/6}, \tag{A.9}$$

where T_r is the relative temperature, $T_\mathrm{r} = T/T_\mathrm{c}$ and $N_\mathrm{Avo} = 6.022 \times 10^{26}\ \mathrm{kmol^{-1}}$.
Dynamic viscosity of the liquid phase [25],

$$\frac{\eta_\mathrm{l}}{\mathrm{Pa\,s}} = \exp\left(-18.345 + \frac{1020.3}{T/\mathrm{K}} + 1.0978\ln\left(\frac{T}{\mathrm{K}}\right) - 6.1 \times 10^{-27}\left(\frac{T}{\mathrm{K}}\right)^{10}\right). \tag{A.10}$$

Thermal conductivity of the gaseous and the liquid phases [26],

$$\frac{k_\mathrm{g}}{\mathrm{W/m\,K}} = \frac{8.757\left(e^{0.0464T_\mathrm{r}} - e^{-0.2412T_\mathrm{r}}\right) + 9.55\left(-0.152T_\mathrm{r} + 1.191T_\mathrm{r}^2 - 0.039T_\mathrm{r}^3\right)}{0.457 \times 10^6 T_\mathrm{c}^{1/6}M^{1/2}p_\mathrm{c}^{-2/3}}, \tag{A.11}$$

$$\frac{k_\mathrm{l}}{\mathrm{W/m\,K}} = \frac{0.1495(1 - T_\mathrm{r})^{0.38}}{T_\mathrm{r}^{1/6}}. \tag{A.12}$$

Surface tension [27],

$$\frac{\sigma}{\mathrm{N/m}} = 5.0573 \times 10^{-2}\left(1 - \frac{T/\mathrm{K}}{408.15}\right)^{1.24412}. \tag{A.13}$$

The enthalpy of vaporization is calculated using Clausius-Clapeyron's equation. The correlations above yield the following values at a temperature of 25 °C and a pressure of 1 bar, or, at the saturation pressure at 25 °C, if appropriate: $\Delta h_\mathrm{vap} = 328.6$ kJ/kg, $v_\mathrm{g} = 0,4153\ \mathrm{m^3/kg}$, $p_\mathrm{sat} = 3.494$ bar, $c_{p,\mathrm{g}} = 1.689$ kJ/kg K, $c_{p,\mathrm{l}} = 2.433$ kJ/kg K, $\eta_\mathrm{g} = 7.733 \times 10^{-6}$ Pa s, $\eta_\mathrm{l} = 1.662 \times 10^{-4}$ Pa s, $k_\mathrm{g} = 0.0164$ W/K m, $k_\mathrm{l} = 0.0957$ W/K m, $\sigma = 9.897$ mN/m.

References

[1] D. I. Petukhov, M. V. Berekchiian, E. S. Pyatkov, K. A. Solntsev, A. A. Eliseev, Experimental and theoretical study of enhanced vapor transport through nanochannels of anodic alumina membranes in a capillary condensation regime, The Journal of Physical Chemistry C 120 (20) (2016) 10982–10990. doi:10.1021/acs.jpcc.6b02971.

[2] D. I. Petukhov, K. S. Napolskii, A. A. Eliseev, Permeability of anodic alumina membranes with branched channels, Nanotechnology 23 (33) (2012) 335601. doi:10.1088/0957-4484/23/33/335601.

[3] H. Rhim, S.-T. Hwang, Transport of capillary condensate, Journal of Colloid and Interface Science 52 (1975) 174–181. doi:10.1016/0021-9797(75)90314-8.

[4] K.-H. Lee, S.-T. Hwang, The transport of condensible vapors through a microporous vycor glass membrane, Journal of Colloid and Interface Science 110 (2) (1986) 544–555. doi:10.1016/0021-9797(86)90407-8.

[5] B. Abeles, L.-F. Chen, J. W. Johnson, J. M. Drake, Capillary condensation and surface flow in microporous vycor glass, Israel Journal of Chemistry 31 (1991) 99–106. doi:10.1002/ijch.199100010.

[6] R. J. R. Uhlhorn, K. Keizer, A. J. Burggraaf, Gas transport and separation with ceramic membranes. Part I. multilayer diffusion and capillary condensation, Journal of Membrane Science 66 (2-3) (1992) 259–269. doi:10.1016/0376-7388(92)87016-Q.

[7] P. Uchytil, R. Petrickovic, S. Thomas, A. Seidel-Morgenstern, Influence of capillary condensation effects on mass transport through porous membranes, Separation and Purification Technology 33 (3) (2003) 273–281. doi:10.1016/S1383-5866(03)00087-X.

[8] E. R. Gilliland, R. F. Baddour, J. L. Russell, Rates of flow through microporous solids, AIChE Journal 4 (1) (1958) 90–96. doi:10.1002/aic.690040117.

[9] P. S. Sidhu, E. L. Cussler, Diffusion and capillary flow in track-etched membranes, Journal of Membrane Science 182 (1-2) (2001) 91–101. doi:10.1016/S0376-7388(00)00546-9.

[10] W. Schneider, Vapor flow through a porous membrane — a throttling process with condensation and evaporation, Acta Mechanica 47 (1) (1983) 15–25. doi:10.1007/BF01176497.

[11] T. Loimer, P. Uchytil, R. Petrickovic, K. Setnickova, The flow of butane and isobutane vapors near saturation through porous Vycor glass membranes, Journal of Membrane Science 383 (2011) 104–115. doi:10.1016/j.memsci.2011.08.035.

[12] T. Loimer, K. Setnickova, R. Petrickovic, P. Uchytil, Flux of isobutane vapors near saturation through multi-layered ceramic membranes, Separation and Purification TechnologyIn preparation.

[13] The MathWorks, Inc., Natick, Massachusetts, United States, MATLAB Release 2017a (2017).

[14] P. Uchytil, T. Loimer, Large mass flux differences for opposite flow directions of a condensable gas through an asymmetric porous membrane, Journal of Membrane Science 470 (2014) 451–457. doi:10.1016/j.memsci.2014.07.055.

[15] R. B. Bird, W. E. Stewart, E. N. Lightfoot, Transport Phenomena, Wiley, 1960.

[16] D. I. Petukhov, A. A. Eliseev, Gas permeation through nanoporous membranes in the transitional flow region, Nanotechnology 27 (8) (2016) 085707. doi:10.1088/0957-4484/27/8/085707.

[17] T. Loimer, Effects of capillarity on a Joule-Thomson process of a fluid near saturation, in: Y. Wang, K. Hutter (Eds.), Trends in Applications of Mathematics to Mechanics. Proc. 14th STAMM, Aug. 22–28, 2004, Seeheim, Germany, 2005, pp. 247–256.

[18] T. Loimer, The flow of saturated vapor with positive Joule-Thomson coefficient through a porous membrane, in: Proceedings of the Fourth European Thermal Sciences Conference, 29th–31st Mar. 2004, Birmingham, UK, no. paper POM1 S14, 2004.

[19] A. Cai, L.-p. Yang, J.-p. Chen, T.-g. Xi, S.-g. Xin, W. Wu, Thermal conductivity of anodic alumina film at (220 to 480) k by laser flash technique, Journal of Chemical & Engineering Data 55 (11) (2010) 4840–4843. doi:10.1021/je100437j.

[20] VDI-Gesellschaft Verfahrenstechnik und Chemieingenieurwesen (Ed.), VDI-Wärmeatlas, 9th Edition, VDI-Verlag, Düsseldorf, 2002. doi:10.1007/978-3-662-10743-0.

[21] J. H. Dymond, K. N. Marsh, R. C. Wilhoit, K. C. Wong, Virial coefficients of pure gases, in: M. Frenkel, K. N. Marsh (Eds.), Virial Coefficients of Pure Gases and Mixtures, Vol. 21A of Landolt-Börnstein. New Series, Group IV: Physical Chemistry, Springer, 2002.

[22] R. C. Wilhoit, K. N. Marsh, X. Hong, N. Gadalla, M. Frenkel, Densities of aliphatic hydrocarbon: Alkanes, in: M. Frenkel, K. R. Hall, K. N. Marsh (Eds.), Thermodynamic Properties of Organic Compounds and Their Mixtures, Vol. 8B of Landolt-Börnstein. New Series, Group IV: Physical Chemistry, Springer, 1996.

[23] J. Dykyj, J. Svoboda, R. C. Wilhoit, M. Frenkel, K. R. Hall, Vapor pressure and antoine constants for hydrocarbon, and sulfur, selenium, tellurium, and halogen containing organic compounds, in: K. R. Hall (Ed.), Vapor Pressure of Chemicals, Vol. 20A of Landolt-Börnstein. New Series, Group IV: Physical Chemistry, Springer, 1999.

[24] R. H. Perry, D. W. Green, J. O. Maloney (Eds.), Perry's Chemical Engineers' Handbook, 7th Edition, McGraw-Hill, 1997.

[25] D. S. Viswanath, T. K. Ghosh, D. H. L. Prasad, N. V. K. Dutt, K. Y. Rani, Viscosity of Liquids, Springer, 2007. doi:10.1007/978-1-4020-5482-2.

[26] R. C. Reid, J. M. Prausnitz, B. E. Poling, The Properties of Gases and Liquids, 4th Edition, McGraw-Hill, 1987.

[27] K. Stephan, H. Hildwein, Recommended data of selected compounds and binary mixtures, Vol. 4 — 1+2 of Chemistry data series, DECHEMA, Frankfurt am Main, 1987.